Title

Controlling Cation-Cation Interactions in Uranyl Coordination Dimers by Varying the Length of the Dicarboxylate Linker

Journal

European Journal of Inorganic Chemistry, 2020(47)

ISSN

1434-1948

Authors

Maurice, Rémi
Dau, Phuong D
Hodée, Maxime
et al.

Publication Date

2020-12-20

DOI

10.1002/ejic.202000840

Peer reviewed

Key Topic: Uranyl Complexes

Controlling Cation-Cation Interactions in Uranyl Coordination Dimers by Varying the Length of the Dicarboxylate Linker

Dr. Rémi Maurice[1,*], Dr. Phuong D. Dau[2], Maxime Hodée[3], Dr. Eric Renault[3], Dr. John K. Gibson[2,*]

[1]SUBATECH, UMR CNRS 6457, IN2P3/IMT Atlantique/Université de Nantes, 4 rue Alfred Kastler, BP 20722, 44307 Nantes Cedex 3, France

[2]Chemical Sciences Division, Lawrence Berkeley National Laboratory, Berkeley, California 94720, United States

[3]CEISAM, UMR CNRS 6230, Université de Nantes, 2 rue de la Houssinière, BP 92208, 44322 Nantes Cedex 3, France

[*]Corresponding authors: rmaurice@subatech.in2p3.fr; jkgibson@lbl.gov

Abstract

The chemistry of linear uranyl(V/VI) dioxo cations, $[O_{yl}\text{-}U\text{-}O_{yl}]^{+/2+}$, is dominated by coordination of uranium in the equatorial plane. Effects of this constraint were evaluated by experiment and theory for gas-phase mixed-valence $U^{V/VI}$ coordination dimers in which uranyl moieties are linked by alkyl dicarboxylates, $[(UO_2^{+})(UO_2^{2+})(OOC\text{-}(CH_2)_{n\text{-}2}\text{-}COO^{2-})_2]^{-}$ (n = 3-12). Faster O_2-addition to dimers with short linkers n = 3 and 4, versus $n \geq 5$, suggests a structural difference. Computed structures with the shortest linkers have bridging dicarboxylates and nearly parallel, non-interacting uranyls. Longer linkers, n = 5-7, accommodate uranyl orientations with distinct U^{V}-U^{VI} end-on cation-cation interactions (CCIs), whereby Lewis base O_{yl} from U^{V} coordinates to the acid U^{VI}, denoted as $U^{V}O_{yl}\cdots U^{VI}$. The dimer structure for n = 8 has a U^{V}-U^{VI} side-on diamond-shape CCI, with $U^{V}O_{yl}\cdots U^{VI}$ and $U^{VI}O_{yl}\cdots U^{V}$ interactions. Addition of O_2 to the n = 4 and 5 dimers yields $[(UO_2^{2+})_2(OOC\text{-}(CH_2)_{n\text{-}2}\text{-}COO^{2-})_2(O_2^{-})]^{-}$, with U^{V} oxidized to U^{VI} and O_2 reduced to O_2^{-}. Whereas O_2 can associate to and oxidize the exposed U^{V} center for dimers with n = 3 and 4, the more crowded U^{V} site in the CCI structures inhibits O_2 addition. The results demonstrate rational structural control of uranyl-uranyl bonding and reactivity in small coordination complexes.

Introduction

A dominant motif in uranium chemistry is the linear dioxo U^{VI} uranyl moiety, UO_2^{2+}.[1-5] Less prevalent reduced uranyl(V), UO_2^{+}, is a key intermediate in such processes as reduction and water oxo-exchange of U^{VI}.[6-10] A central characteristic of uranyl chemistry is coordination of the U center by donor ligands in the exposed equatorial plane perpendicular to the linear O_{yl}-U-O_{yl} moiety. Among the plethora of uranyl compounds, uranyl-organic frameworks (UOFs) belong to the broader class of metal-organic frameworks (MOFs) in which metal centers are linked by ditopic or polytopic coordinating ligands.[11-16] Large functionalized pores of MOFs present opportunities for use in gas adsorption and storage, catalysis, and ion sensing.[17-19] Although potential applications such as photocatalysis, and metal ion adsorption and detection, among others, have stimulated interest in UOFs,[20-25] their structural diversity alone provides motivation for fundamental inquiry.

Uranyl carboxylate coordination complexes have been studied in solution and solid phases for more than 50 years.[26-31] The ability of dicarboxylates to bind strongly to two metal centers has resulted in extensive application as the linker in MOFs. The versatility of dicarboxylate (and polycarboxylate) linkers for assembling metal ions results from their wide range of sizes and geometries, and functional groups that can be located between the coordination sites. The carboxylate moieties are sufficiently discrete to enable rationally targeted coordination structures and properties. Functionalities incorporated into the spacers will ultimately decorate the MOF pores.[32] Among reported UOF structure types are double chain with 1,4-naphthalene dicarboxylates,[33] giant cages with calixarene carboxylates,[34] topological nets with a tetrahedral carboxylate,[35] extended three-dimensional polymeric with citrate,[36] and tube-like with 1,4-phenylene dicarboxylate.[37]

Several UOFs with aliphatic α,ω-dicarboxylate linkers have been reported, from the groups of Thuéry,[38-42] Cahill,[43-45] and others.[46-47] The compositions of these elementary uranyl(VI) UOFs can simplistically be represented as $(UO_2^{2+})(C\mathit{n}^{2-})$ where $C\mathit{n}^{2-}$ designates the aliphatic α,ω-dicarboxylate anion with a total of *n* carbon atoms, $C\mathit{n}^{2-} \equiv [OOC\text{-}[(CH_2)_{n-2}]\text{-}COO]^{2-}$. Actual UOF compositions are generally more complex than suggested by this nomenclature, such as when additional ions disrupt the stoichiometry of U^{VI}:$C\mathit{n}^{2-}$ = 1:1. Typically, $(UO_2^{2+})(C\mathit{n}^{2-})$ UOFs exhibit structures that feature uranyl monomers, dimers or larger assemblages tethered together in chains or planar arrays. Uranyl succinate hydrate, $[(UO_2^{2+})(C4^{2-})]\bullet H_2O$, has sheets of uranyl moieties.[47]

The next longer linker, n = 5 (glutarate), results in a structure with uranyl dimers connected in chains that interconnect to form sheets.[43] Longer more flexible linkers such as n = 12 and 13 allow more diverse structural arrangement of the uranyl moieties, and also more structural disorder.[41] The UOF structure with the very long n = 15 linker suggests key effects of the counterion for long linkers, and for compositions that are not simple charge-balanced $(UO_2^{2+})(C_n^{2-})$.[40] Remarkable helix structures were found for some uranyl complexes with C_n^{2-} for $n \geq 9$.[42] In these "triple-stranded helicate" structures, two uranyl moieties are linked by three C_n^{2-}. It was concluded that linkers shorter than n = 9 cannot support such a connectivity of two uranyl units due to the constraint of uranium-coordination in the equatorial plane. Although the field of UOFs has focused on U^{VI}, Mazzanti characterized a coordination polymer with uranyl(V) units linked by potassium cations interacting with the O_{yl} oxo-groups;[48] as the linkers are not organic this is a uranyl *inorganic* framework (UIF).

The role of U^V as a key intermediate in processes such as reduction of U^{VI} to U^{IV} highlights the significance of mixed-valence uranyl(V/VI) complexes,[49-51] particularly those with well-defined interactions between U^V and U^{VI} centers. Although it does not possess a dioxo uranyl(V) center, a stunning mixed-valence complex is a star-shaped $U^{V/VI}$ oxo-cluster supported by benzoate ligands.[52] A more directly pertinent case, also from Mazzanti, is a uranyl(V/VI) complex that exhibits a so-called "cation-cation" interaction (CCI).[53] In such a CCI a Lewis base O_{yl}, typically from a uranyl(V), datively binds to an acidic U^V center, a situation denoted as $U^VO_{yl}\cdots U^V$, or to a even more acidic U^{VI} center, denoted as $U^VO_{yl}\cdots U^{VI}$. The first identified actinyl CCIs in solution were not for uranyl but rather for neptunyl(V), $Np^VO_{yl}\cdots Np^V$.[54] The two essential types of CCIs exhibited by actinyls, end-on and side-on, are shown for uranyl in Scheme 1.

The intersection of the realms of UOFs and CCIs has yielded intriguing crystal structures, particularly in the last decade. Loiseau reported a structure in which octanuclear uranyl assemblies exhibiting CCIs are linked by phthalates ,[55] and a UOF in which uranyl chains with CCIs are assembled into sheets by citrate.[56] In another UOF, a terephthalate links dimers in which the two uranyls are bound together by a CCI.[57] When reporting a uranyl UOF with dimer CCIs, in this case with biphenyl dicarboxylate linkers, Cahill refreshingly acknowledged that this discovery, like most U^{VI}-U^{VI} CCIs, was serendipitous.[58] A final example may be better described as a coordination polymer rather than a UOF because instead of acting as linkers, the coordinating bipyridine ligands prevent the CCI-linked uranyl chains from coalescing.[59]

Our involvement in the field of UOFs employs model gas-phase species for elucidation at a fundamental level, while also providing insights relevant to development of condensed-phase UOF chemistry. The general utility and versatility of gas-phase studies has been established in many realms, such as organometallic chemistry and C-H bond activation.[60-67] Examples of gas-phase contributions to uranium chemistry include oxo-exchange of uranyl with water,[68] a nitrosyl complex,[69] a peroxide dimer,[70] and an "extreme" CCI.[71] Stand-alone computational studies have assessed stabilities of elementary CCIs in gas-phase uranyl dimers.[72-73]

In the present work, electrospray ionization (ESI) of solutions containing uranyl and dicarboxylates was employed to generate gas-phase uranyl coordination complexes for reactivity studies in a quadrupole ion trap mass spectrometer (QIT-MS). Among the species produced were uranyl dimers supported by aliphatic α,ω-dicarboxylates, $C\mathit{n}^{2-} \equiv [OOC\text{-}[(CH_2)_{\mathit{n}-2}]\text{-}COO]^{2-}$. We report a combined experimental and computational study of dimers $[(UO_2^{+})(UO_2^{2+})(C\mathit{n}^{2-})_2]^{-}$ for n = 3-12, with particular focus on model dimers with linkers succinate (n = 4) and glutarate (n =5). The experimental results indicate a structure and reactivity break for dimers with these linker lengths, which are sufficiently small to be tractable by density functional theory (DFT) involving conformational searches with several spins and charges for distinct fragments, as well as multiple possible 3D space arrangements. The reliability of the computations is bolstered by accord with kinetics for oxidation of $U^{V/VI}$ mixed-valence dimers to $U^{VI/VI}$ superoxides by adsorption of O_2. The reported gas-phase dimers exhibit the following characteristics that are directly relevant to assembly and properties of condensed phase coordination complexes: 1) Structures are determined by the length of the dicarboxylate linker $C\mathit{n}^{2-}$; 2) Different linkers result in uranyl moieties that are either non-interacting or connected through a CCI; 3) Structural constraints imposed by the CCIs result in oxidation by long-range electron transfer from U^{V} to O_2, via an intermediate U^{VI} site; and 4) A transition from no CCIs for short linkers (n = 3-4), to end-on CCIs for intermediate linkers (n = 5-7), to side-on CCIs for long linkers ($\mathit{n} \geq 8$) governs uranyl reactivity in a controlled manner. The appearance of these characteristics in elementary gas-phase species presents opportunities for fundamental understanding and control of processes such as directed assembly of UOFs, creation of CCIs, and intramolecular charge transfer.

Experimental Details

Caution! The uranium-238 isotope used in this work is radioactive and must be handled with appropriate precautions in a special radiological laboratory.

The general experimental approach has been described previously.[74] Anionic uranyl complexes were produced by ESI of an ethanol solution containing uranyl chloride (0.1 mM from a 10 mM pH 2 stock solution) and dicarboxylic acid, HOOC-$(CH_2)_{n-2}$-COOH (0.1 mM H_2C*n* with *n* = 3, 4, 5, 6, 7, 8, 9, 10 or 12; Sigma-Aldrich). Ions prepared by ESI are accumulated in the quadrupole ion trap (QIT) of an Agilent 6340 mass spectrometer that has been modified as described previously.[75] Ions in the QIT can undergo ion-molecule reactions at ~300 K[76] by applying a reaction time of up to 10 s. The following experimental parameters were used: solution flow rate, 60 µL/h; nebulizer gas pressure, 12 psi; capillary voltage offset and current, 4850 V and 208 nA; end plate voltage offset and current, -500 V and 450 nA ; dry gas flow rate, 3 l/min; dry gas temperature, 325 °C; capillary exit, -300 V; skimmer, -47.6 V; octopole 1 and 2 DC, -10.4 V and -1.8 V; octopole RF amplitude, 300 Vpp; lens 1 and 2, 15.0 V and 100.0 V; trap drive, 64.3. Nitrogen gas for nebulization and drying was supplied from the boil-off of a liquid nitrogen Dewar. The background water pressure in the ion trap is estimated as ~10^{-6} Torr; reproducibility of hydration rates of $UO_2(OH)^+$ established that the water pressure was constant to within <10%.[74] The helium buffer gas pressure in the QIT is constant at ~10^{-4} Torr.

Computational Approach

Geometry optimizations of bare complexes

The ground state geometries of bare complexes $[(UO_2^+)(UO_2^{2+})(Cn^{2-})_2]^-$ (*n* = 3–8), as well as $[UO_2]^+$, $[UO_2]^{2+}$, O_2 and O_2^-, were determined with closed-shell spin-restricted and open-shell spin-unrestricted density functional theory (DFT and UDFT), using various starting geometries and spins (total and local). Except for the *n* = 7 and *n* = 8 cases, for which only one or two characteristic minimum energy structures were sought, reported in Supporting Information (SI) are at least all low-energy structures within a 10 kJ/mol range, in terms of "pure" electronic energy, E, enthalpy at 298 K, H (298 K), and/or Gibbs free energy, G (298 K). For each reported structure the spin state or configuration is given in SI (for DFT or UDFT calculations, respectively).

When applicable, local oxidation states were inferred from atomic spin densities on the uranium sites: ~0 for U^{VI} and ~1 for U^{V} in UDFT calculations, which are practically independent of the underlying charge scheme. For mixed-valence U^V/U^{VI} complexes, spin densities of ~0.5 for the two U sites would indicate "delocalization" as in class III compounds in the Robin-Day classification.[77] As the closed-shell *S* = 0 DFT calculation for the ground state of $[UO_2]^{2+}$ cannot

generate a U^V site, U^{VI} necessarily results there. In all reported mixed-valence complexes, one U^V site and one U^{VI} site were clearly identified, leading to the notation $[(UO_2^+)(UO_2^{2+})(Cn^{2-})_2]^-$. The assignments implied by this notation were initially inferred from compositions/charges, and subsequently computationally confirmed.

Geometry optimizations of complexes with O_2

For two or more metal centers, addition of O_2 may give rise to several spin states/configurations and structures for each initial structure of the bare complex.[78] We focused on O_2 addition to bare complexes with compositions $[(UO_2^+)(UO_2^{2+})(C4^{2-})_2]^-$ and $[(UO_2^+)(UO_2^{2+})(C5^{2-})_2]^-$, as their structures suggest they provide a reasonable explanation for the experimental results. We also considered bare $[UO_2]^+$ and $[UO_2]^{2+}$ for comparison.

For the O_2 adducts, UDFT calculations were performed. As all other situations lead to an odd number of unpaired electrons, only addition of O_2 to bare UO_2^{2+} could lead to a closed-shell compound, which does not happen since the lowest-energy solution has $M_S = 1$ (see SI). Having only open-shell solutions after addition of O_2, atomic spin densities are key for assigning the U oxidation state and charge on O_2. If the sum of the spin densities on the two O atoms is ~2, then it is triplet neutral O_2; if the sum is ~1 it is superoxide O_2^- (O_2^+ is dismissed as too high in energy); if the sum is ~0 then additional information such as atomic charges and O-O distance is required to assign it as a O_2^{2-} or singlet O_2.

Computational details

All calculations were performed with the *Gaussian 09* program package.[79] The hybrid generalized gradient approximation PBE0 exchange-correlation functional[80-81] was used, as in previous work on actinyl nitrates.[82-83] The choice of a hybrid density functional is typical for such actinide complexes. The uranium atoms have been described by means of the small-core scalar-relativistic ECP60MWB energy-consistent pseudopotential[84] with the (14s13p10d8f6g)/[10s9p5d4f3g] contracted basis set.[85] All-electron split-valence basis sets[86-87] were used for the other atoms: def2-SVPD, *i.e.* (8s5p2d)/[4s3p2d], for O, def2-SVP, *i.e.* (7s4p1d)/[3s2p1d], for C and def2-SV, *i.e.* (4s)/[2s], for H. The *grid = ultrafine* keyword of Gaussian was employed to set up the integration grid. The minimum-energy structures were characterized by the absence of an imaginary vibrational frequency. When several conformers may coexist, the Gibbs free energy for individual conformers is reported; the free energy of the ensemble of conformers was not computed. For the reaction energies we focus on differences of

the "pure" electronic energies E, for simplicity and in accord with the objective of explaining the experimental observations. The spin-orbit coupling (SOC) stabilization of the ground state due to the presence of a U^V site has been neglected, but this is not anticipated to have a significant effect when comparing energies for similar reactions. Except for addition of O_2 to UO_2^{2+}, for which the oxidation state is U^{VI} throughout, all reported reaction energies are expected to suffer from a similar U^V SOC bias of ~30 kJ/mol,[88-89] which is considered when relevant in the comparisons.

Results and Discussion

Preparation of uranyl coordination dimers

Representative anion ESI mass spectra for solutions containing uranyl and one of several α,ω-dicarboxylic acids H_2Cn (n = 3-10 or 12) are shown in Figure 1 for n = 4 and n = 9, and in SI Figure S1 for other values of n. Observed mononuclear uranyl species include the following, where moieties and oxidation states $U^VO_2^+$ or $U^{VI}O_2^+$ are assigned based on compositions and charges: (a) $[(UO_2^{2+})(Cl^-)_3]^-$; (b) $[(UO_2^+)(Cn^{2-})]^-$; (c) $[(UO_2^{2+})(Cl^-)(Cn^{2-})]^-$; (d) $[(UO_2^{2+})(HCn^-)(Cn^{2-})]^-$; and (e) $[(UO_2^{2+})(Na^+)(Cn^{2-})_2]^-$. The chlorine constituent in (a) and (c) is from uranyl chloride; the sodium in (e) is an ubiquitous contaminant. Uranyl chloride species (a) and coordination complex (c) are apparent for the uranyl-$C3^{2-}$ solution. For the longer dicarboxylates, all coordination complexes (b)–(e) are observed in various abundances. The abundance of complex (d), for example, is generally greater for larger values of n. It should be noted that ESI is a complicated dynamic process such that the abundances of coordination complexes do not necessarily directly indicate their intrinsic stabilities, nor their concentrations in solution. With this caveat, we note that higher abundances of complex (d) for longer linkers may reflect more facile complexation of both ends of the same dicarboxylate to a single uranyl, at least in the gas phase.

Our primary interest is in the dinuclear uranyl species apparent in the ESI mass spectra (Fig. S1), (f) $[(UO_2^+)(UO_2^{2+})(Cn^{2-})_2]^-$ and (g) $[(UO_2^{2+})_2(Cl^-)(Cn^{2-})_2]^-$. The abundance of species (f) was barely above the detection limit for n = 3, substantially greater for n = 4-8, and highest for n = 9, 10 and 12. In analogy with the effect suggested above for mononuclear complexes, these relative abundances may reflect more facile tethering of two uranium centers by the longer dicarboxylates. Complex (g) corresponds to oxidation of the U^V center in dimer (f) to U^{VI} by chloride, which is analogous to what occurs in the superoxide complexes discussed below.

Observed reactions of dimers $[(UO_2^+)(UO_2^{2+})(Cn^{2-})_2]^-$

Although relative ESI abundances of the uranyl dicarboxylate complexes may reflect structures and stabilities, such correlations are at best qualitative, at worst misleading, and generally speculative. We instead turn to gas-phase bimolecular ion-molecule reactions under thermal conditions (~300 K) to compare the dimers. Each of the dimers $[(UO_2^{+})(UO_2^{2+})(C_n^{2-})_2]^-$ (n = 3-10 or 12) was isolated in the ion trap and exposed to background gases for a variable reaction time, followed by determination of the reaction products. The background gas pressure was indeterminate but constant to within 10%, with the primary reactive constituents being O_2 and H_2O.[74] Representative reaction results are shown in Figure 2 for the n = 4, 5, 6 and 7 dimers, all of which spontaneously capture O_2. We tentatively present this process by reaction (1), where oxidation of U^V to U^{VI} by formation of a superoxide is supposed based on previous results for O_2 addition to U^V complexes.[74] These formulations are computationally corroborated below. The n = 5 and 6 dimers further add H_2O according to reaction (2). It is not known whether the product of reaction (2) is a physisorption hydrate, as suggested by the chosen formulation, or rather a chemisorption hydroxide. The latter, which would presumably have H_2O and a U-O oxo converted to two U-OH moieties, as in $[(UO_2^{2+})(UO(OH)_2^{2+})(C_n^{2-})_2(O_2^{-})]^-$, would be an unusual disruption of uranyl and is perhaps less likely than the hydrate alternative. It is noted that conversion of the superoxide moiety to hydroxides would seemingly imply an unrealistic oxidation state higher than U^{VI}, as in $[(UO_2^{2+})(UO_2^{3+})(C_n^{2-})_2(OH^{-})_2]^-$.

$$[(UO_2^{+})(UO_2^{2+})(C_n^{2-})_2]^- + O_2 \rightarrow [(UO_2^{2+})_2(C_n^{2-})_2(O_2)]^- \quad (1)$$

$$[(UO_2^{2+})_2(C_n^{2-})_2(O_2^{-})]^- + H_2O \rightarrow [(UO_2^{2+})_2(C_n^{2-})_2(O_2^{-})(H_2O)]^- \quad (2)$$

The results in Figure 2 show that the rate for O_2-addition reaction (1) is faster for n = 4 and slower for n = 6, both relative to n = 5. Detailed kinetics results are in SI, with a summary shown in Figure 3 as a plot of the measured rate of O_2 addition at nearly constant O_2 pressure. As no reaction was observed for the n = 8, 9, 10 and 12 dimers, the upper limit for these rates is estimated as 0.005 s^{-1}. The rates for the n = 3 and 4 dimers are substantially higher than for those with longer dicarboxylates. Notably, the rate decreases from 1.49 s^{-1} for n = 4 to 0.22 s^{-1} for n = 5, which suggests an essential change in structure there. A focus of the computational effort was to understand the origins of the change in reactivity indicated by the results in Figure 3.

Water addition reaction (2) also reveals significant differences between dimers. Water addition was observed only for the n = 5 and 6 dimers; it is evident from Figure 2 that the rate is significantly faster for n = 6. Another key observation is that H_2O addition only occurs after O_2

addition, as in reaction (2), and is not observed for any of the bare dimers $[(UO_2^+)(UO_2^{2+})(Cn^{2-})_2]^-$. This result suggests that hydration and/or hydrolysis is somehow enhanced by the O_2 sorption site, which would be consistent with conversion of the superoxide to hydroxides that was dismissed above as implying an unrealistically high uranium oxidation state. As the computational focus was the O_2-addition reactions, the (interesting) phenomenon of water addition is not further pursued here.

Structures of dimers $[(UO_2^+)(UO_2^{2+})(Cn^{2-})_2]^-$ (n = 3-8)

The difference in reactivity between the linker n = 3-4 dimers, versus those with linkers n = 5 and longer, stimulated interest in structures of bare dimers $[(UO_2^+)(UO_2^{2+})(Cn^{2-})_2]^-$ and O_2-adduct dimers $[(UO_2^{2+})_2(Cn^{2-})_2(O_2)]^-$. Several minimum-energy structures were computed for bare dimers having n = 3-6; reported are all structures found within 10 kJ/mol of that with lowest energy (i.e. energy E, enthalpy H (298 K), or free energy G (298 K)). Also reported are selected structures with higher energy, and a few for n = 7 and 8. The bare and O_2-adduct dimer structures are summarized in Table 1 and shown in Figures 4-6. In all bare dimers, the two U sites are clearly distinguished as one in oxidation state +V with atomic spin density of ~1, indicating a UO_2^+ moiety, and the other +VI with spin density ~0, indicating a UO_2^{2+}. The DFT results do not suggest class III mixed-valence complexes according to the classification of Robin and Day,[90] but rather localization of the "extra" electron on the U^V site. Further assignment as class I or II was not pursued due to the complex potential energy surfaces. It is noted that electron transfer between U^V and U^{VI} sites is expected to be inhibited by requisite structural changes.

For bare dimers with n = 3, two very similar C_s symmetry structures were found within ~5 kJ/mol of one another. These are denoted $\mathbf{A_{br}}$ and $\mathbf{A_{br}}'$ where the subscript "br" indicates a structure in which carboxylate oxygen atoms O_{br} form a "bridge" between the uranyl moieties. Such bridging structures are differentiated below from those for $n \geq 5$ that exhibit CCIs. Representative structure $\mathbf{A_{br}}$, shown in Figure 4, has two nearly parallel uranyl moieties (U^V and U^{VI}) linked by two O_{br}. The U-O_{yl} distances for the two uranyl moieties, 1.76 Å and 1.80 Å, are characteristic of U^{VI} and U^V, respectively.[91] For the n = 4 dimers the two identified structures, $\mathbf{B_{br}}$ and $\mathbf{B_{br}}'$, which belong to symmetry point groups C_s and C_2, differ only by a slight variation in linker arrangement and are within 1 kJ/mol of one another. Representative structure $\mathbf{B_{br}}$ is shown in Figure 4. Structures $\mathbf{B_{br}}$ and $\mathbf{B_{br}}'$, like $\mathbf{A_{br}}$ and $\mathbf{A_{br}}'$, have two nearly parallel U^{VI}/U^V uranyl moieties with characteristic U^V-O_{yl} and U^{VI}-O_{yl} distances, and linked by two carboxylate O_{br}

atoms. In summary, the bare dimers for n = 3 and 4 exhibit similar bridging structures, with U^{V} coordinated by bidentate carboxylates that form a bridge to U^{VI}, which is additionally coordinated by monodentate carboxylates; the result is fourfold equatorial coordination of both U^{V} and U^{VI}.

For the dimer with the next longer linker, n = 5, the three obtained structures are denoted $\mathbf{C_{br}}$, $\mathbf{C_{br}}'$ and $\mathbf{C_{cc}}$. The first two very similar bridging structures are within 0.1 kJ/mol (E) of one another, while the third structure, displaying a CCI, is ~7 kJ/mol lower in energy. Structure $\mathbf{C_{br}}$, shown in Figure 5, is analogous to the bridging structures for linkers n = 3 and 4, with nearly parallel uranyl moieties linked by two O_{br}. In structure $\mathbf{C_{cc}}$, in lieu of bridging carboxylate O_{br} atoms, an O_{yl} from U^{V} forms a dative bond to U^{VI} in an end-on CCI configuration (Scheme 1). The CCI distance, $U^{V}O_{yl}\cdots U^{VI}$, is 2.26 Å, which is comparable to the U-$O_{carbonyl}$ distances, and slightly shorter than $U^{V}O_{yl}\cdots U^{V}$ CCI distance of 2.37 Å in a condensed phase complex.[6] The $U^{V}O_{yl}\cdots U^{VI}$ CCI angle in $\mathbf{C_{cc}}$ is 143°, which is significantly less than the ideal end-on angle of 180°. Whereas $\mathbf{C_{cc}}$ has the lowest energy E of the three structures for n = 5, $\mathbf{C_{br}}'$ has the lowest free energy G (298 K), though by less than 2 kJ/mol (Table 1). Possible systematic computational errors at this level of theory are illustrated by the variation in the fine result with the exchange-correlation functional reported for a uranyl nitrate complex[92]. Considering possible errors and the similar energies of the found structures, we do not contend to have identified the correct energetic ordering for the bare n = 5 dimer. Rather, we suppose that nearly isoenergetic structures $\mathbf{C_{b}}$, $\mathbf{C_{br}}'$ and/or $\mathbf{C_{cc}}$ are all feasible; considerations discussed below suggest that structure $\mathbf{C_{cc}}$ is dominant in the experiments.

The identification of low-energy bridging and CCI structures for the dimer with n = 5, versus only bridging for n = 3 and 4, is in accord with the original hypothesis of a structure change around this linker length. The structures in Figures 4 and 5 suggest that short linkers n = 3 and 4 cannot support a CCI like $\mathbf{C_{cc}}$ for n = 5. Computations for bare dimers with n = 6-8 further demonstrate the importance of CCIs in structures with relatively long linkers. For the n = 6 dimer, the two found structures, $\mathbf{D_{br}}$ and $\mathbf{D_{cc}}$, are shown in Figure 6. Structure $\mathbf{D_{br}}$ is analogous to the bridging structures for n = 3-5, with nearly parallel uranyl moieties linked by bridging dicarboxylates, while $\mathbf{D_{cc}}$ is analogous to CCI structure $\mathbf{C_{cc}}$. Whereas structures $\mathbf{C_{br}}$ and $\mathbf{C_{cc}}$ for n = 5 are nearly isoenergetic, for the next longer n = 6 linker CCI structure $\mathbf{D_{cc}}$ is substantially lower energy than bridging structure $\mathbf{D_{br}}$ (ΔE = 29.3 kJ/mol). For even longer linker n = 7, we obtained structure $\mathbf{E_{br/cc}}$ shown in Figure 6. The subscript "br/cc" denotes a structure with both a bridging O_{br} and a CCI, though the addition of a monodentate carboxylate at the expense of a bidentate one

results in the same equatorial coordination of 4 in $\mathbf{E_{br/cc}}$ as in CCI-only structures like $\mathbf{D_{cc}}$. For the dimer with n = 8, two very similar CCI structures within 4.1 kJ/mol of one another were found, with representative structure $\mathbf{F_{cc}}$ shown in Figure 6. Structure $\mathbf{F_{cc}}$ is remarkable in exhibiting a side-on CCI with O_{yl} atoms from both U^{V} and U^{VI} acting as donors to the other U center. The two $UO_{yl}\cdots U$ CCI angles in this complex, 103° and 114°, are somewhat larger than the ideal side-on CCI angle of 90° (Scheme 1). CCI structure $\mathbf{F_{cc}}$ is also distinctive among those reported here in having all four carboxylate moieties bidentate, with the result that both U centers exhibit relatively high fivefold equatorial coordination, to yield overall a less usual coordination of seven around both U centers.

Except for $\mathbf{F_{cc}}$, all the reported structures have at least one monodentate carboxylate. In contrast, in solid compounds with two carboxylate groups coordinated to uranyl, both are typically bidentate.[93] Furthermore, in gas phase complexes with uranyl coordinated by three carboxylates, they are either all bidentate, or two bidentate and one mondentate.[94] Reduced carboxylate denticity in the molecular dimers reported here suggests geometric constraints imposed by the dicarboxylate backbone that preclude optimal coordination. In contrast to these dimers, extended solid state polynuclear structures with short dicarboxylate linkers do not suffer from the constraint of only two coordinated uranium centers, and they can thus accommodate fully bidentate coordination. An example for n = 4 is UOF [(UO_2)(C4)•H_2O] in which the uranyl moieties assemble with fully bidentate carboxylate coordination.[47] A closer analogy to the molecular dimers constructed and considered here is the dinuclear uranyl helicate structure with n = 9 azelate linkers connecting two uranyl centers reported by Thuéry and Harrowfield.[42] In this exquisite structure, fully bidentate coordination of all three linking dicarboxylates results in sixfold equatorial coordination of uranyl. The n = 9 linkers are adequately long for the O_{yl}-U-O_{yl} uranyl moieties in the helicate to adopt a configuration in which they are co-linear, with two O_{yl} atoms pointing directly towards one another without undue repulsion. In contrast, for the molecular dimers reported here the nearly parallel side-by-side orientation of the two O_{yl}-U-O_{yl} in structures such as $\mathbf{C_{br}}$ and $\mathbf{D_{br}}$ is evidently necessary to similarly minimize O_{yl}-O_{yl} repulsive interactions. In alternative CCI structures like $\mathbf{C_{cc}}$ and $\mathbf{D_{cc}}$, rotation of the uranyl(V) relative to uranyl(VI) results in the $U^{V}O_{yl}\cdots U^{VI}$ bonding interaction. As the longest linker computationally assessed here was n = 8, we recognize the possibility that longer linkers such as n = 9 azelate might support molecular dimer structures with directly opposing uranyl moieties like in the helicate. However, in the

absence of a third dicarboxlate linker, to provide sixfold equatorial uranyl coordination as in the helicate, the side-on CCI interaction in structures such as **F_{cc}** provide the maximum coordination, which likely renders such CCI configurations as the most energetically favorable.

The U-U distances in most of the dimer structures are in the range of 3.9 – 4.2 Å, which is too long for significant U-U bonding. However, the U^{V}-U^{VI} distance is significantly shorter for the *n* = 7 and 8 CCI dimer structures (Table 1), specifically 3.69, 3.50 and 3.49 Å for **$E_{br/cc}$**, **F_{cc}**, and **F_{cc}´**, respectively. Although these distances may still be too long for significant U-U bonding, they are only moderately longer than the distance of 3.43 Å for which a U-U effective magnetic interaction has been reported,[95] though it does not involve a U^{VI} site as in our dimers but instead two U^{V} sites.

The two types of structures identified for the bare dimers, bridging and CCI, suggest structural control by the length of the dicarboxylate linker, with CCI structures favored as the linker length increases. For the shortest linkers, *n* = 3 and 4, only bridging structures like **A_{br}** and **B_{br}** were found at low energies. These linkers are evidently too short to accommodate both effective carboxylate coordination and reorientation of the uranyl moieties needed for a CCI. For intermediate length linker *n* = 5, bridging and CCI structures have very similar energies. This linker is sufficiently long to allow the highly non-parallel uranyl CCI orientation in structure **C_{cc}**. The next longer linker, *n* = 6, is results in a CCI significantly lower energy than a bridging structure. As both of the *n* = 6 structures **D_{cc}** and **D_{br}** have fourfold equatorial uranyl coordination, the higher stability of the CCI structure suggests more favorable bonding for the $U^{V}O_{yl}\cdots U^{VI}$ CCI bond, versus the additional U-$O_{carboxylate}$ bond in the bridging structure. The structure found for *n* = 7 also has an end-on type CCI, in addition to a single bridging carboxylate oxygen, O_{br}. The longest linker for which computations were performed, *n* = 8, allows the uranyl moieties to orient in a side-on CCI configuration. In this *n* = 8 dimer all four carboxylate moieties are bidentate, and both U have the maximum of fivefold equatorial coordination.

Structures and energies of O_2-adducts $[(UO_2^{2+})_2(Cn^{2-})_2(O_2)]^-$ (n = 4,5)

The apparent shift from bridging structures for short linkers (*n* = 3 and 4) to CCI structures for longer linkers ($n \geq 5$) suggests that this change may explain the observed break in reactivity around this linker length (Figure 3). As the bare dimers having *n* = 4 and *n* = 5 exhibit the essential structural features—bridging and CCI—and are sufficiently small to be computationally tractable, they are considered as suitable models for O_2 addition. Reaction (1) was thus computationally

assessed for $[(UO_2^+)(UO_2^{2+})(C4^{2-})_2]^-$ structure **B_{br}**, and $[(UO_2^+)(UO_2^{2+})(C5^{2-})_2]^-$ structures **C_{br}** and **C_{cc}**. The resulting structure **$B_{br}(O_2)$** of O_2-adduct $[(UO_2^{2+})_2(C4^{2-})_2(O_2)]^-$ is shown in Figure 4; structures **$C_{br}(O_2)$** and **$C_{cc}(O_2)$** of adduct $[(UO_2^{2+})_2(C5^{2-})_2(O_2)]^-$ are shown in Figure 5; reaction (1) energies are in Table 2.

Oxygen addition to n = 4 dimer structure **B_{br}** occurs at the U^V site to yield **$B_{br}(O_2)$**, with an increase in equatorial coordination of the reactive site from fourfold U^V in **B_{br}** to sixfold U^{VI} in **$B_{br}(O_2)$**, while the coordination of the spectator U^{VI} site remains fourfold throughout. The U^V-O_{yl} distance of 1.80 Å in **B_{br}** contracts to a typical U^{VI}-O_{yl} distance of 1.75 Å in **$B_{br}(O_2)$**. The O-O distance of 1.29 Å in **$B_{br}(O_2)$** is characteristic of a superoxide O_2^-,[96] as confirmed by summed atomic spin densities of ~0 on the two O atoms, as well as on both U^{VI} sites. In further accord with assignment of **$B_b(O_2)$** as a superoxide, the energy for reaction (1a) for the n = 4 dimer, ΔE = -164 kJ/mol, is in the range of -143 to -195 kJ/mol previously reported for oxidative addition of O_2 to mononuclear anion complexes $[(UO_2^+)(X^-)_2]^-$ to yield superoxides $[(UO_2^{2+})(X^-)_2(O_2^-)]^-$ (X = OH, F, Cl, Br, I).[97] The O_2 association reaction (1a) is exothermic, as required based on its spontaneous occurrence under low-energy conditions. Furthermore, O_2 association to the exposed U^V site in **B_{br}** should be facile, with the rate expected to be limited only by the ability of the nascent hot adduct **$B_{br}(O_2)^*$** to collisionally cool to **$B_{br}(O_2)$**, rather than dissociate to **B_{br}** and O_2.

Addition of O_2 to structures **C_b** and **C_{cc}** for n= 5 was found to result in structures **$C_b(O_2)$** and **$C_{cc}(O_2)$** shown in Figure 5. As for **B_{br}**, O_2 addition to **C_{br}** occurs at the exposed U^V site with formation of superoxide in which U^V is oxidized to U^{VI} with an increase from fourfold to sixfold coordination. We refer to oxidation processes such as those identified for **B_{br}** and **C_{br}** as "direct" to reflect **that** addition of O_2 is directly to the U^V site that is oxidized to U^{VI}. Alternative "indirect" mechanisms discussed below for other structures proceed by O_2 addition to a U^{VI} site, with U^V thus oxidized to U^{VI} indirectly. It is expected that direct addition of O_2 to **B_{br}** and **C_{br}**, as well as **D_{br}** and other bridging structures, should be facile and exhibit similar kinetics. Accordingly, the experimental observation of a significantly slower rate for the dimer with n = 5 versus n = 4 suggests different types of structures for the bare reactant dimers, which would specifically exclude **C_{br}** (at least partially). We surmise that the operative structure for n = 4 is **B_{br}**, as per the computations, whereas for n = 5 it is CCI structure **C_{cc}**, which is nearly isoenergetic with the alternative bridging structures. The next computational goal was to assess whether CCI structure **C_{cc}** actually accounts for relatively slow O_2 addition kinetics for the dimer with n = 5.

For the **$C_{cc}(O_2)$** structure shown in Figure 5 the O-O distance of 1.29 Å, and the atomic spin densities, again indicate a superoxide with oxidation of U^V to U^{VI}. The CCI $U^{VI}O_{yl}\cdots U^{VI}$ distance in **$C_{cc}(O_2)$**, 2.40 Å, is longer than the CCI $U^VO_{yl}\cdots U^{VI}$ distance in **C_{cc}** (2.26 Å) but shorter than for a condensed phase U^{VI}-U^{VI} CCI (2.48 Å).[58] Compared with CCI $U^{VI}O_{yl}\cdots U^{VI}$, a stronger and shorter $U^VO_{yl}\cdots U^{VI}$ interaction is expected based on more basic character of donor O_{yl} atoms in uranyl(V) versus uranyl(VI). Even without consideration of mechanistic details for O_2 addition, greater complexity for **C_{cc}** (versus **C_{br}**) is indicated by the change from equatorial coordination of fourfold for both U^V and U^{VI} in **C_{cc}** to fivefold in **$C_{cc}(O_2)$**. Fivefold coordination in the CCI adduct cannot result from simple addition of a side-on η^2-O_2 to one of the two U centers as occurs for **C_{br}**, but instead requires U-O bond reorganization that should result in slower kinetics, as was observed. Conceptions for transformation of **C_{cc}** to both **$C_{cc}(O_2)$** and **$C_{br}(O_2)$** are shown schematically in Figure 7. In "direct" mechanism (a), O_2 associates directly to U^V, which is oxidized to U^{VI}, with reorganization of the carboxylate coordination by cleavage of U(α)-O(6) and formation of U(β)-O(12) (green line and arrow in Figure 7). As the two perspectives of the **C_{cc}** structure in Figure 5 suggest, "direct" association of O_2 to U^V in **C_{cc}** may be inhibited by the local coordination environment, which is more congested than U^V in **C_{br}**. This supposition of inhibited "direct" association of O_2 to U^V in **C_{cc}** is supported by geometry optimizations that show placing O_2 near the U^V site of **C_{cc}** does not obviously lead to **$C_{cc}(O_2)$**.

Like process (a), alternative processes (b) and (c) in Figure 7 for "indirect" O_2 addition to U^{VI} in **C_{cc}** are substantially exothermic. Indirect O_2 addition yields **$C_{cc}(O_2)$** by mechanism (b) or **$C_{br}(O_2)$** by (c). Necessary bond breakings and makings (green lines and arrows) and electron transfers (purple arrows) are identified in Figure 7. In (b), the CCI donor $U^V(\alpha)$ in **C_{cc}** becomes the acceptor $U^{VI}(\alpha)$ in **$C_{cc}(O_2)$** in a CCI; i.e., $U^V(\alpha)O_{yl}(2)\cdots U^{VI}(\beta)$ is replaced by $U^{VI}(\beta)O_{yl}(7)\cdots U^{VI}(\alpha)$. Oxidation occurs by intramolecular electron transfer is from $U^V(\alpha)$ to $U^{VI}(\beta)$ and from $U^{VI}(\beta)$ to O_2. Although electron transfer between metal centers mediated by an oxo bridge is well established,[98] such oxidation over a CCI bridge is distinctive. As in (b), in indirect mechanism (c) the U^{VI}/U^V CCI is disrupted. In this case it is not replaced by a U^{VI}/U^{VI} CCI; instead a bridging carboxylate structure is formed. As indicated in Figure 7, transformation (c) involves cleavage and formation of multiple U-O bonds, which should present substantial kinetic barriers.

The possible mechanisms schematically summarized in Figure 7 do not intend to provide a reliable or detailed rendition of the transformation of $[(UO_2^+)(UO_2^{2+})(C5^{2-})_2]^-$ to $[(UO_2^{2+})_2(C5^{2-}$

$)_2(O_2)]^-$. Rather, the intent is to convey that O_2 addition to CCI structures like **C_{cc}** almost certainly encounters kinetic barriers greater than for addition to bridging structures like **B_{br}** and **C_{br}**. These barriers essentially result from obstruction of "direct" association to the U^V CCI donor site that is ultimately oxidized, and from the structural reorganization needed to achieve a low-energy product conformation after addition to the U^{VI} site. As a result of this evaluation, the observed decrease in dimer reactivity between $n = 4$ and $n = 5$ is reasonably attributed as due to structure **C_{cc}** for $n = 5$. As CCI structures become increasingly important for longer linkers, $n \geq 6$, it is furthermore reasonable to surmise that barriers associated with this structural motif generally inhibit O_2 addition and result in the relatively slow kinetics that were observed for all dimers having $n \geq 5$.

A final aspect of the O_2-adduct dimers that warrants attention is relative energies of some of the structures. For the bare dimer with linker $n = 5$, CCI structure **C_{cc}** is at nearly the same energy as bridging structures **C_{br}** and **C_{br}'**. However, for the corresponding O_2-adduct, CCI structure **$C_{cc}(O_2)$** is 48 kJ/mol higher energy than bridging structures **$C_{br}(O_2)$** and **$C_{br}(O_2)'$**. Upon formation of **$C_{cc}(O_2)$**, energy is provided by the creation of a U^{VI}-O_2^- bonding interaction; also, CCI $U^VO_{yl}\cdots U^{VI}$, with a CCI bond distance of 2.26 Å, is replaced by CCI $U^{VI}O_{yl}\cdots U^{VI}$, with bond distance 2.40 Å. These distances indicate that the latter CCI is weaker, which reflects the less basic character of O_{yl} in U^{VI} versus U^V. As the created superoxide bonding is common to both the bridging and CCI structures, the decrease in bonding efficacy of the CCI should at least partly account for stabilization of the bridging vs. CCI structures for the O_2 adduct. A result of this stabilization of bridging structures is that the lowest energy reaction pathway for **C_{cc}** is to **$C_{br}(O_2)$**, pathway (c) in Figure 7. However, as the discussion above suggests, the actual operative reaction pathway is likely governed by kinetic barriers imposed by the CCI structure of **C_{cc}**, not necessarily by achieving an overall reaction energy minimum. For example, a process such as (c) in Figure 7 may be too convoluted to be realistically accessible.

Addition of O_2 to bare uranyl(V) and uranyl(VI)

For comparison with the dimer results, O_2 addition to bare uranyl(V) and uranyl(VI) was computed, with the resulting reaction energies in Table 2 and product structures in Figure 8. The computed U-O_{yl} bond distances for the bare linear uranyl ions are 1.74 Å for $[UO_2]^+$ and 1.68 Å for $[UO_2]^{2+}$. Chemisorption of O_2 by $[UO_2]^+$ produces $[(UO_2^{2+})(O_2^-)]^+$ with a typical superoxide O-O distance of 1.27 Å, the U-O_{yl} distance shortened by ~0.02 Å relative to bare $[UO_2]^+$, the O_{yl}-U-O_{yl} angle bent to 174.6°, and two U-O distances of 2.25 Å. As the uranium center in $[UO_2]^{2+}$

cannot practically oxidize further, O_2 addition yields physisorption adduct $[(UO_2^{2+})(O_2)]^{2+}$ having O_2 in an end-on monodentate coordination mode with a relatively long U-O bond distance of 2.43 Å. This adduct exhibits a short O-O distance of 1.19 Å, which is within ~0.02 Å of that in free O_2, a U-O_{yl} distance elongated by ~0.01 Å relative to bare $U^{VI}O_2^{2+}$, and an O_{yl}-U-O_{yl} angle only slightly bent to 177.4°.

The energy computed for physisorption of O_2 by $[UO_2]^{2+}$ is -106 kJ/mol. This ion-dipole interaction energy is significantly less negative than the -278 kJ/mol reported for addition of H_2O to $[UO_2]^{2+}$,[68] which reflects the absence of a permanent dipole moment for O_2. The ΔE computed for oxidative chemisorption of O_2 to $[UO_2]^+$ without considering spin-orbit coupling, -83 kJ/mol, is actually much less negative than for physisorption by $U^{VI}O_2^{2+}$. Indeed, as mentioned above, the SOC stabilizes U^V sites while minimally affecting the U^{VI} ones. Based on previous reports, we estimate that the actual relative energies for U^V species are more favorable than those computed here without SO by ~30 kJ/mol.[88-89] This correction yields an estimated ΔE ≈ -53 kJ/mol for oxidative addition of O_2 to $[UO_2^+]$, which is only half as negative as computed for O_2 physisorption to $[UO_2^{2+}]$. Thus, the dication-O_2 electrostatic interaction is evidently much stronger than formation of a uranyl-superoxide bond concomitant with oxidation from U^V to U^{VI}.

Association of O_2 to bare $[UO_2]^+$, and to $\mathbf{C_{br}}$ according to reaction (1c) in Table 2, corresponds to simple oxidative addition with minimal structural rearrangement. Assuming a similar spin-orbit correction for both processes, oxidative addition to $\mathbf{C_{br}}$ is computed to be more exothermic by ~80 kJ/mol. This difference might be partly due to less positive charge on the U^V center in an anion complex such as $\mathbf{C_{br}}$. An alternative but practically equivalent perspective is that the U^V center is partially reduced due to ligand electron donation in $\mathbf{C_{br}}$. In general, less positive and/or partially reduced U^V centers in anion complexes should exhibit more exothermic electron donation to a neutral O_2 to yield U^{VI} superoxide complexes, as found here.

Conclusions

Solution ESI yielded gas-phase dinuclear uranyl coordination complexes $[(UO_2^+)(UO_2^{2+})(C\mathit{n}^{2-})_2]^-$ where $C\mathit{n}^{2-}$ is an aliphatic α,ω-dicarboxylate linker with n = 3-12 carbon atoms. Differing rates of O_2 addition suggested structural variations with the length of $C\mathit{n}^{2-}$, most notably a rate decrease between n = 4 and n = 5. Computations indicate that low-energy structures for the dimers with n = 3 and n = 4 have two nearly parallel non-interacting uranyl moieties in which the U^V site is exposed for facile oxidative addition of O_2. The slightly longer and more

flexible n = 5 linker enables a CCI structure in which the more basic U^{V}-O_{yl} is the Lewis donor and U^{VI} the acceptor. In this CCI configuration the U^{V} site is congested and inaccessible for direct addition of O_2, which instead occurs at U^{VI} with "indirect" oxidation of U^{V} by intramolecular electron transfer and substantial structural reorganization. A $U^{V}O_{yl}\cdots U^{VI}$ CCI is characteristic of the structures for dimers with linkers $n \geq 5$. The change in dimer reactivity between $n = 4$ and $n = 5$ is attributed to a structural shift from non-interacting uranyls with exposed U^{V} to CCI structures in which the U^{V} site is inaccessible for direct O_2 addition. For the dimer with $n = 8$, and presumably longer linkers, slow kinetics are attributed to a side-on CCI structure.

The complementary experimental and computational results demonstrate control of the proximity, orientation and interaction between uranyl moieties in simple dinuclear coordination complexes, from nearly parallel and non-interacting for short linkers (n = 3 and 4), to end-on CCIs for intermediate linkers (n = 5-7), and to side-on CCIs for long linkers (n = 8, and possibly longer). Extremely short linkers such as oxalate (n = 2) might stabilize structures with quasi-parallel uranyl moieties sufficiently close for the U^{V}-U^{VI} interaction to yield intermediate valence $U^{+5.5}$. In contrast to closed shell configuration $[Rn]5f^{0}$ of U^{VI}, the $[Rn]5f^{1}$ of Np^{VI} and $[Rn]5f^{2}$ of Pu^{VI} have 5f electrons that can participate in bonding; coordination dimers containing neptunyl and plutonyl present opportunities to induce actinide-actinide bonding. Although gas-phase coordination dimers may not directly reflect speciation and structures in condensed phase, they do demonstrate and elucidate controlled linking of actinyl moieties.

CCI structures like $\mathbf{C_{cc}}$ for dimer $[(UO_2^{+})(UO_2^{2+})(C5^{2-})_2]^{-}$ render the U^{V} site sterically congested and unavailable for facile attachment of O_2 to form a superoxide. Aa a result, oxidation of U^{V} is expected to proceed by O_2 association to U^{VI}, with (concerted) electron transfer across the CCI, expressed as $U^{V}O_{yl}\rightarrow U^{VI}\rightarrow O_2$. Electron transfer from U^{V} to U^{VI} via intervening ligands such as hydroxide and fluoride has been characterized previously.[50] The elementary U^{V} to U^{VI} electron transfer process identified here is distinctive in being driven by the approach of an oxidant molecule, specifically O_2, to U^{VI}, and with the transfer occurring over a CCI concomitant with its structural reorganization.

Acknowledgements

The experimental work was fully supported by the U.S. Department of Energy, Office of Science, Office of Basic Energy Sciences, Chemical Sciences, Geosciences, and Biosciences Division,

Heavy Element Chemistry Program, at Lawrence Berkeley National Laboratory under Contract DE-AC02-05CH11231 (PDD and JKG). The computational work was carried out using HPC resources from CCIPL (“Centre de Calcul Intensif des Pays de la Loire”).

Supporting Information

Complete reference 76. ESI mass spectra. Kinetics results for O_2 addition to dimers. Computed molecular structures and energies.

Table 1. Summary of computed structures and relative energies.[a]

Species	Structure[b]	SPG[c]	CN_{eq}[d]	U-U distance / $U\text{-}O_{CCI}\text{-}U$ angle[e]	E (kJ/mol)	G (298K) (kJ/mol)
$[(UO_2^{+})(UO_2^{2+})(C3^{2-})_2]^{-}$	$\mathbf{A_{br}}$	C_s	4/4	4.08	0	0
″	$\mathbf{A_{br}}'$	C_s	4/4	4.08	5.1	6.4
$[(UO_2^{+})(UO_2^{2+})(C4^{2-})_2]^{-}$	$\mathbf{B_{br}}$	C_s	4/4	4.11	0	0.3
″	$\mathbf{B_{br}}'$	C_2	4/4	4.13	0.2	0
$[(UO_2^{+})(UO_2^{2+})(C5^{2-})_2]^{-}$	$\mathbf{C_{cc}}$	C_1	4/4	3.96 / 143	0	1.6
″	$\mathbf{C_{br}}$	C_s	4/4	4.14	7.4	1.3
″	$\mathbf{C_{br}}'$	C_2	4/4	4.15	7.5	0
$[(UO_2^{+})(UO_2^{2+})(C6^{2-})_2]^{-}$	$\mathbf{D_{cc}}$	C_1	4/4	4.03 / 150	0	0
″	$\mathbf{D_{br}}$	C_1	4/4	4.14	29.3	25.3
$[(UO_2^{+})(UO_2^{2+})(C7^{2-})_2]^{-}$	$\mathbf{E_{br/cc}}$	C_1	4/4	3.69 / 125	-	-
$[(UO_2^{+})(UO_2^{2+})(C8^{2-})_2]^{-}$	$\mathbf{F_{cc}}$	C_1	5/5	3.50 / 114 / 103	0	0
″	$\mathbf{F_{cc}}'$	C_1	5/5	3.49 / 113 / 103	4.1	3.0
$[(UO_2^{2+})_2(C4^{2-})_2(O_2^{-})]^{-}$	$\mathbf{B_{br}(O_2)}$	C_s	4/6	4.15	0	0.7
″	$\mathbf{B_{br}(O_2)}'$	C_2	4/6	4.17	0.2	0
$[(UO_2^{2+})_2(C5^{2-})_2(O_2^{-})]^{-}$	$\mathbf{C_{cc}(O_2)}$	C_1	5/5	3.91 / 134	48.0	59.3
″	$\mathbf{C_{br}(O_2)}$	C_s	4/6	4.18	0	1.0
″	$\mathbf{C_{br}(O_2)}'$	C_2	4/6	4.19	0.1	0

[a] Energies relative to the lowest energy structure found for a given composition.
[b] Subscript "cc" denotes a CCI structure; "br" denotes a bridging carboxylate structure.
[c] Symmetry Point Group.
[d] Equatorial coordination numbers of the two U atoms (naturally, $CN_{ax} = 2$ in all the cases). The longest U-O distance assigned as a coordination bond is 2.64 Å for the CCI in $\mathbf{F_{cc}}$ (Figure 6).
[e] U-U distance in Å, and $U\text{-}O_{CCI}\text{-}U$ angle(s), where applicable, in degrees.

Table 2. Energies for addition of O_2 to uranyl dimers, reaction (1), and to bare uranyl.

Reaction	ΔE (kJ/mol)
(1a) $\mathbf{B_{br}} + O_2 \rightarrow \mathbf{B_{br}(O_2)}$	-164[a]
(1b) $\mathbf{C_{cc}} + O_2 \rightarrow \mathbf{C_{cc}(O_2)}$	-109[b]
(1c) $\mathbf{C_{br}} + O_2 \rightarrow \mathbf{C_{br}(O_2)}$	-165[b]
(1d) $\mathbf{C_{cc}} + O_2 \rightarrow \mathbf{C_{br}(O_2)}$	-157[b]
(1e) $\mathbf{C_{br}} + O_2 \rightarrow \mathbf{C_{cc}(O_2)}$	-117[b]
$[UO_2]^+ + O_2 \rightarrow [(UO_2^{2+})(O_2^-)]^+$	-83[c]
$[UO_2]^{2+} + O_2 \rightarrow [(UO_2^{2+})(O_2)]^{2+}$	-106

[a]Energy with $\mathbf{B_{br}}'$ or $\mathbf{B_{br}(O_2)}'$ instead of $\mathbf{B_{br}}$ or $\mathbf{B_{br}(O_2)}$ are the same within 1 kJ/mol.
[b]Energy with $\mathbf{C_{br}}'$ or $\mathbf{C_{br}(O_2)}'$ instead of $\mathbf{C_{br}}$ or $\mathbf{C_{br}(O_2)}$ are the same within 1 kJ/mol.
[c]Applying an estimate for the spin-orbit correction yields a value of ca. -53 kJ/mol.

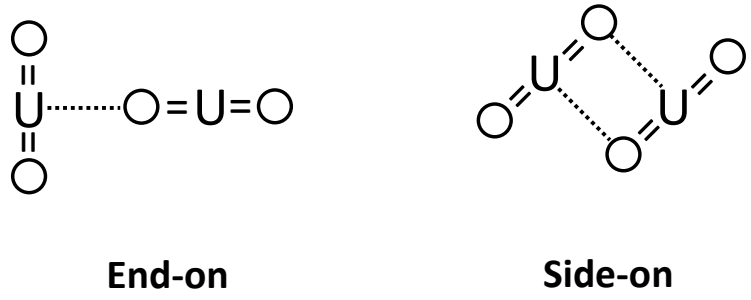

Scheme 1. The two idealized types of uranyl CCI.

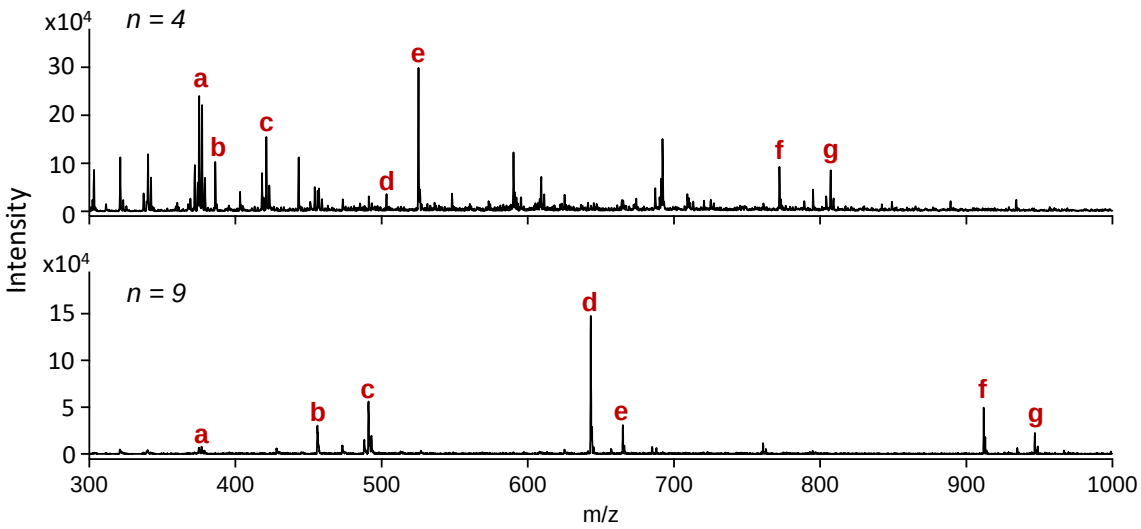

Figure 1. Negative mode ESI mass spectra for the solutions of uranyl chloride and dicarboxylic acid H_2Cn in a 1:1 concentration ratio for n = 4 (top) and n = 9 (bottom). The following peaks corresponding to uranyl-containing species are indicated by labels: (a) $[(UO_2^{2+})(Cl^-)_3]^-$; (b) $[(UO_2^+)(Cn^{2-})]^-$; (c) $[(UO_2^{2+})(Cl^-)(Cn^{2-})]^-$; (d) $[(UO_2^{2+})(HCn^-)(Cn^{2-})]^-$; (e) $[(UO_2^{2+})(Na^+)(Cn^{2-})_2]^-$; (f) $[(UO_2^+)(UO_2^{2+})(Cn^{2-})_2]^-$; and (g) $[(UO_2^{2+})_2(Cl^-)(Cn^{2-})_2]^-$. The presence of Na-containing species is attributed to contamination. Other ESI mass spectra are in Supporting Information.

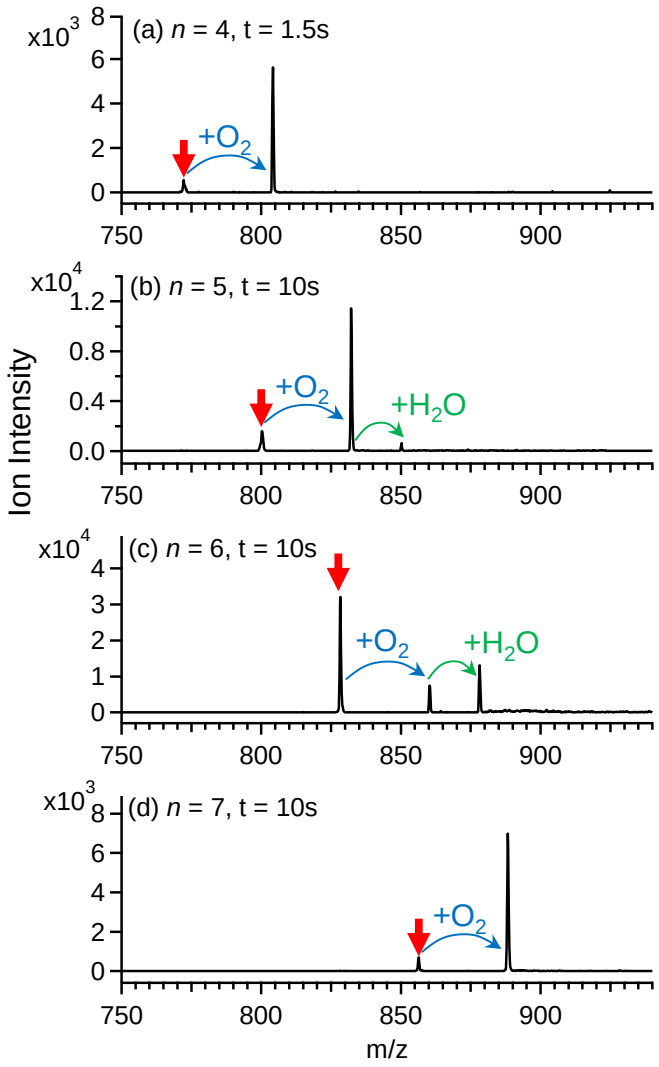

Figure 2. Mass spectra acquired after reaction for time t of dimers $[(UO_2^{+})(UO_2^{2+})(C_n^{2-})_2]^{-}$ (indicated by red arrows) with background gases (O_2 and H_2O). (a) n = 4, t = 1.5 s; (b) n = 5, t = 10 s; (c) n = 6, t = 10 s; (d) n = 7, t = 10 s. The addition of H_2O following O_2 for dimers n = 5 and n = 6, was the only water-addition observed among all of the studied dimers.

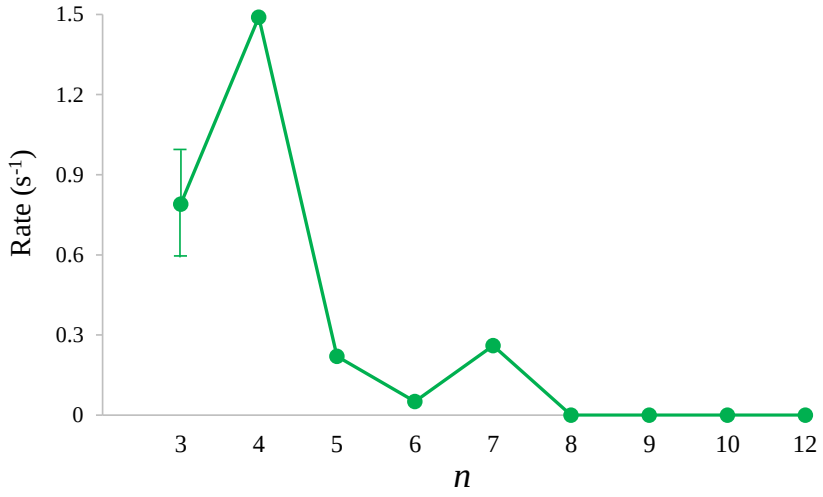

Figure 3. Plot of pseudo-first order rates for O_2 addition to uranyl dicarboxylate dimers $[(UO_2^{+})(UO_2^{2+})(Cn^{2-})_2]^{-}$ to yield $[(UO_2^{2+})_2(Cn^{2-})_2(O_2^{-})]^{-}$. The rate for n = 3 is from a single measurement with the indicated error. Other rates are for at least two measurements with the uncertainty given by the size of the circle. No reaction was detected for n = 8, 9, 10 and 12. Because the O_2 pressure is constant to ≤10% the rates indicate relative reaction efficiencies.

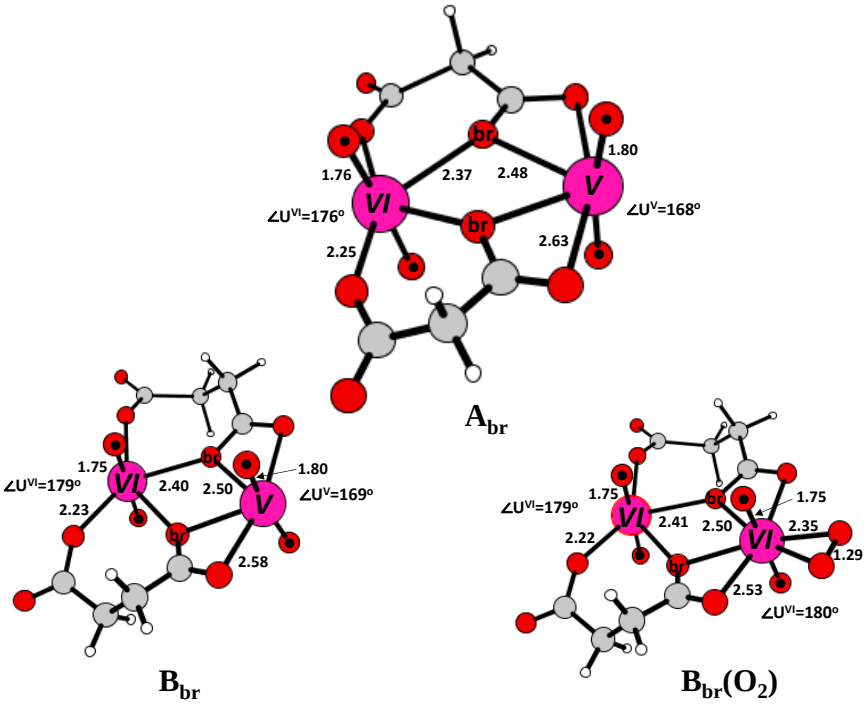

Figure 4. Computed structures **A_{br}** for species $[(UO_2^{+})(UO_2^{2+})(C3^{2-})_2]^{-}$, **$B_{br}$** for $[(UO_2^{+})(UO_2^{2+})(C4^{2-})_2]^{-}$, and **$B_{br}(O_2)$** for $[(UO_2^{+})(UO_2^{2+})(C4^{2-})_2(O_2)]^{-}$. Pink = U; red = O; grey = C; light grey = H. Uranyl O_{yl} are identified by black dots, and bridging O atoms by "br". U oxidation states +V or +VI are indicated. Selected bond distances are given in Å. Uranyl angles $\angle[O_{yl}\text{-}U^{VI}\text{-}O_{yl}]$ ($\angle U^{VI}$) and $\angle[O_{yl}\text{-}U^{V}\text{-}O_{yl}]$ ($\angle U^{V}$) are in degrees.

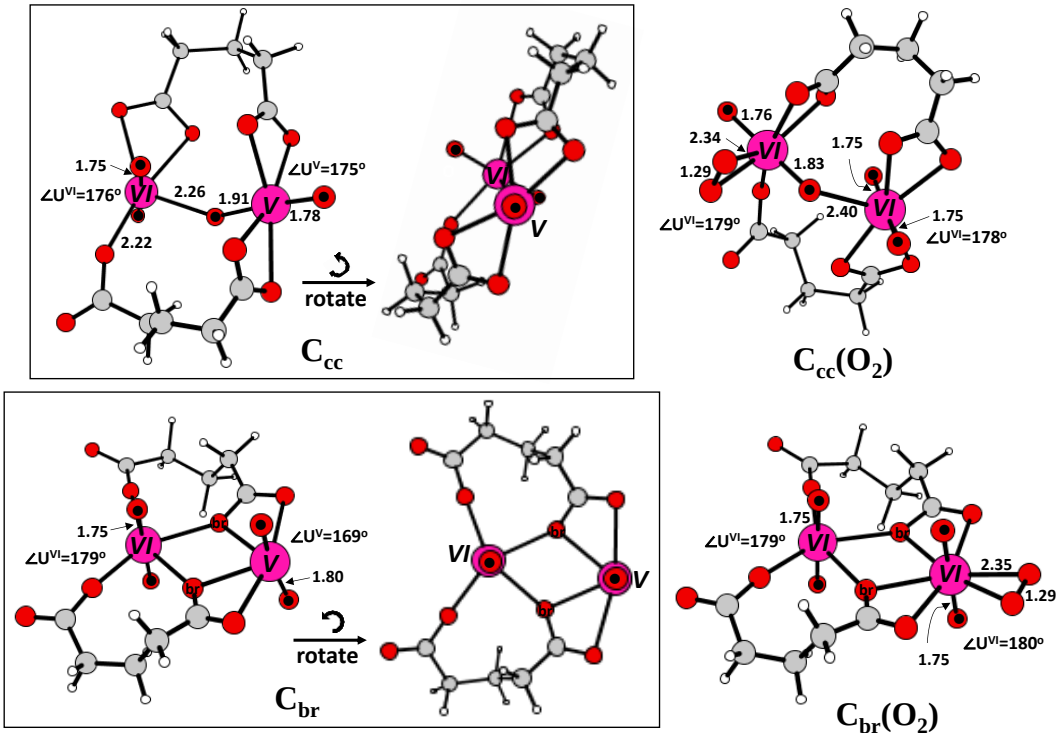

Figure 5. Structures **C_{cc}** and **C_{br}** (two perspectives of both) for species $[(UO_2^{+})(UO_2^{2+})(C5^{2-})_2]^{-}$, and **$C_{cc}(O_2)$** and **$C_{br}(O_2)$** for $[(UO_2^{+})(UO_2^{2+})(C5^{2-})_2(O_2)]^{-}$. Pink = U; red = O; grey = C; light grey = H. Uranyl O_{yl} are identified by black dots, and bridging O atoms by "br". U oxidation states +V or +VI are indicated. Selected bond distances are given in Å. Uranyl angles $\angle[O_{yl}\text{-}U^{VI}\text{-}O_{yl}]$ ($\angle U^{VI}$) and $\angle[O_{yl}\text{-}U^{V}\text{-}O_{yl}]$ ($\angle U^{V}$) are in degrees.

.

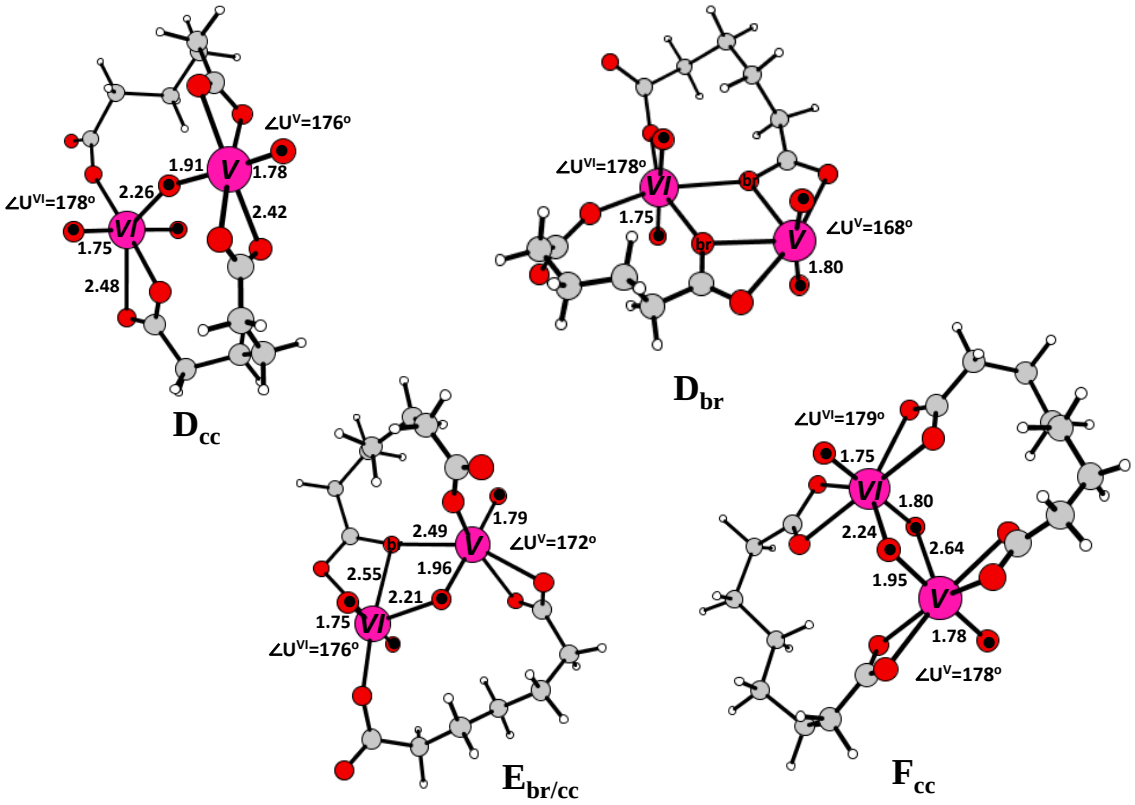

Figure 6. Computed structures **D_{cc}** and **D_{br}** for species $[(UO_2^{+})(UO_2^{2+})(C6^{2-})_2]^{-}$; **$E_{br/cc}$** for $[(UO_2^{+})(UO_2^{2+})(C7^{2-})_2]^{-}$; and **$F_{cc}$** for $[(UO_2^{+})(UO_2^{2+})(C8^{2-})_2]^{-}$. Pink = U; red = O; grey = C; light grey = H. Uranyl O_{yl} are identified by black dots, and bridging O atoms by "br". U oxidation states +V or +VI are indicated. Selected bond distances are given in Å. Uranyl angles $\angle[O_{yl}\text{-}U^{VI}\text{-}O_{yl}]$ ($\angle U^{VI}$) and $\angle[O_{yl}\text{-}U^{V}\text{-}O_{yl}]$ ($\angle U^{V}$) are in degrees.

.

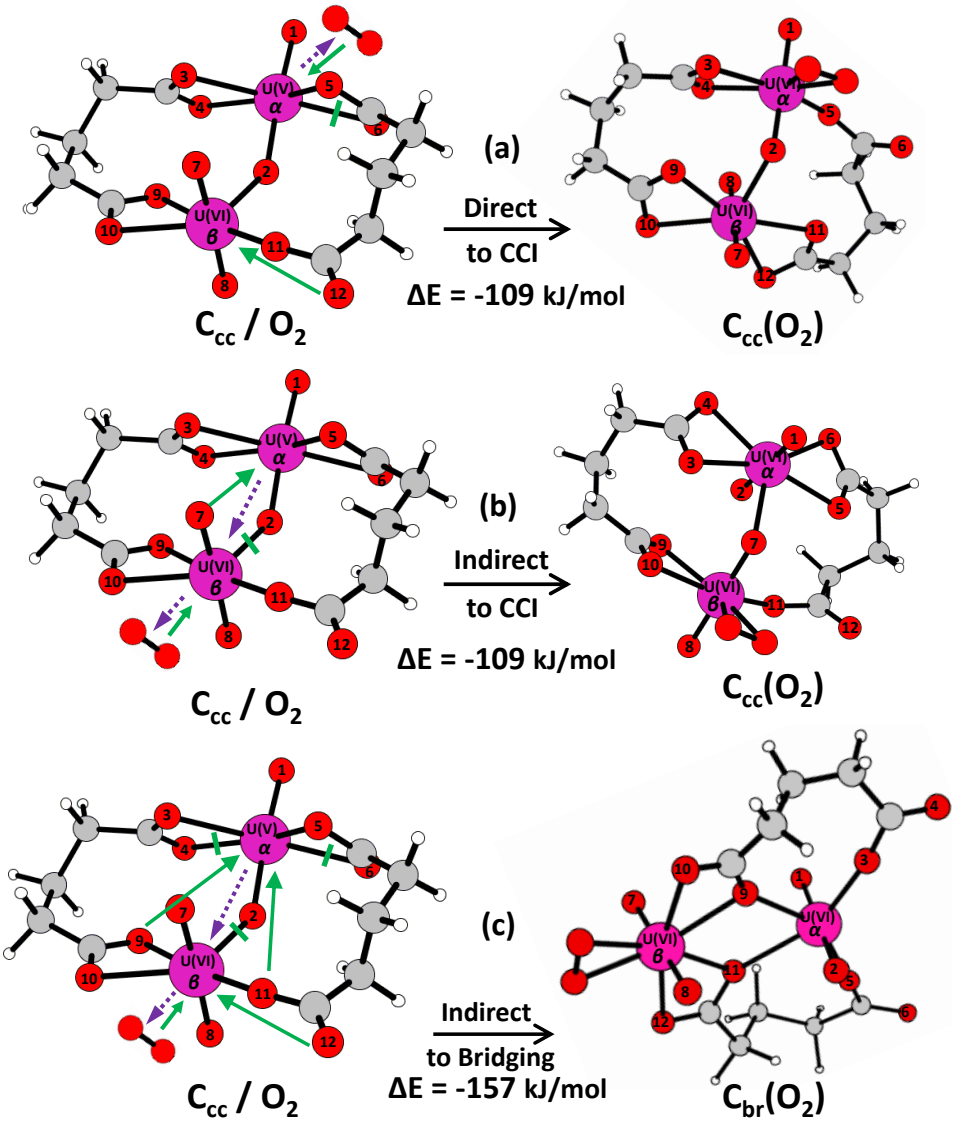

Figure 7. Proposed mechanisms for addition of O_2 to $\mathbf{C_{cc}}$ structure of $[(UO_2^{+})(UO_2^{2+})(C5^{2-})_2]^{-}$, to yield $[(UO_2^{+})(UO_2^{2+})(C5^{2-})_2(O_2)]^{-}$: (a) to $\mathbf{C_{cc}(O_2)}$ by Direct association to U^{V}; (b) to $\mathbf{C_{cc}(O_2)}$ by Indirect association to U^{VI}; (c) to $\mathbf{C_{br}(O_2)}$ by Indirect association to U^{VI}. Green line = bond cleaves; green arrow = bond forms; purple arrow = electron transfer. Direct association (a) is sterically hindered.

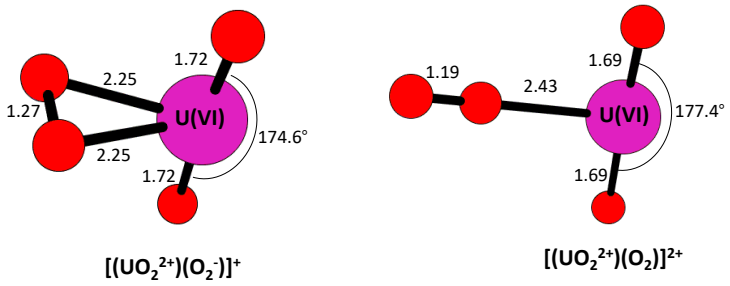

Figure 8. Computed structures for O_2 addition to uranyl(V) and uranyl(VI) to yield uranyl(VI). Left: Superoxide $[(UO_2^{2+})(O_2^{-})]^{+}$ from addition to UO_2^{+}; Right: Adduct $[(UO_2^{2+})(O_2)]^{2+}$ from addition to UO_2^{2+}. Bond distances are in Å; O_{yl}-U-O_{yl} angles are in degrees. The corresponding U-O_{yl} distances are 1.74 Å for bare $U^{V}O_2^{+}$ and 1.68 Å for bare $U^{VI}O_2^{2+}$.

TOC Graphic

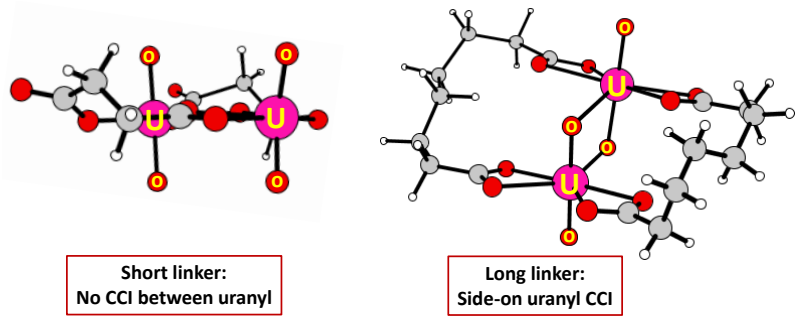

Control of cation-cation interactions (CCIs) in dinuclear uranyl coordination complexes is achieved by adjusting the length of dicarboxylate linkers. Whereas short linkers impose nearly-parallel uranyl orientation to minimize repulsive interactions, longer linkers allow for U-O dative bonding in a CCI oriented either end-on or side-on. The CCI configurations render the U(V) center inaccessible, thereby inhibiting oxidative addition of O_2.

References

[1] S. Ahrland, *Acta Chem Scand* **1949**, *3*, 374-400.
[2] S. P. McGlynn, J. K. Smith, *J Mol Spectrosc* **1961**, *6*, 188-198.
[3] R. G. Denning, *Struct Bond* **1992**, *79*, 215-276.
[4] D. L. Clark, S. D. Conradson, R. J. Donohoe, D. W. Keogh, D. E. Morris, P. D. Palmer, R. D. Rogers, C. D. Tait, *Inorg Chem* **1999**, *38*, 1456-1466.
[5] S. P. McGlynn, W. C. Neely, J. K. Smith, *J Chem Phys* **1961**, *35*, 105-116.
[6] G. Nocton, P. Horeglad, J. Pecaut, M. Mazzanti, *J Am Chem Soc* **2008**, *130*, 16633-16645.
[7] V. Mougel, P. Horeglad, G. Nocton, J. Pecaut, M. Mazzanti, *Chem-Eur J* **2010**, *16*, 14365-14377.
[8] P. L. Arnold, J. B. Love, D. Patel, *Coordin Chem Rev* **2009**, *253*, 1973-1978.
[9] T. W. Hayton, G. Wu, *Inorg Chem* **2008**, *47*, 7415-7423.
[10] J. L. Brown, C. C. Mokhtarzadeh, J. M. Lever, G. Wu, T. W. Hayton, *Inorg Chem* **2011**, *50*, 5105-5112.
[11] M. Eddaoudi, D. B. Moler, H. L. Li, B. L. Chen, T. M. Reineke, M. O'Keeffe, O. M. Yaghi, *Accounts Chem Res* **2001**, *34*, 319-330.
[12] J. Kim, B. L. Chen, T. M. Reineke, H. L. Li, M. Eddaoudi, D. B. Moler, M. O'Keeffe, O. M. Yaghi, *J Am Chem Soc* **2001**, *123*, 8239-8247.
[13] T. K. Kim, K. J. Lee, M. Choi, N. Park, D. Moon, H. R. Moon, *New J Chem* **2013**, *37*, 4130-4139.
[14] B. Masci, P. Thuéry, *Cryst Growth Des* **2008**, *8*, 1689-1696.
[15] M. B. Andrews, C. L. Cahill, *Chem Rev* **2013**, *113*, 1121-1136.
[16] K. X. Wang, J. S. Chen, *Accounts Chem Res* **2011**, *44*, 531-540.
[17] H. Furukawa, K. E. Cordova, M. O'Keeffe, O. M. Yaghi, *Science* **2013**, *341*, 974.
[18] Y. S. Kang, Y. Lu, K. Chen, Y. Zhao, P. Wang, W. Y. Sun, *Coordin Chem Rev* **2019**, *378*, 262-280.
[19] B. M. Connolly, M. Aragones-Anglada, J. Gandara-Loe, N. A. Danaf, D. C. Lamb, J. P. Mehta, D. Vulpe, S. Wuttke, J. Silvestre-Albero, P. Z. Moghadam, A. E. H. Wheatley, D. Fairen-Jimenez, *Nat Commun* **2019**, *10*.
[20] Z. T. Yu, Z. L. Liao, Y. S. Jiang, G. H. Li, G. D. Li, J. S. Chen, *Chem Commun* **2004**, 1814-1815.
[21] Y. N. Hou, X. T. Xu, N. Xing, F. Y. Bai, S. B. Duan, Q. Sun, S. Y. Wei, Z. Shi, H. Z. Zhang, Y. H. Xing, *ChemPlusChem* **2014**, *79*, 1304-1315.
[22] J. Ai, F. Y. Chen, C. Y. Gao, H. R. Tian, Q. J. Pan, Z. M. Sun, *Inorg Chem* **2018**, *57*, 4419-4426.
[23] W. Liu, J. Xie, L. M. Zhang, M. A. Silver, S. Wang, *Dalton Trans* **2018**, *47*, 649-653.
[24] P. Thuéry, Y. Atoini, J. Harrowfield, *Dalton Trans* **2020**, *49*, 817-828.
[25] J. A. Ridenour, M. H. Schofield, C. L. Cahill, *Cryst Growth Des* **2020**, *20*, 1311-1318.
[26] K. S. Rajan, A. E. Martell, *J Inorg Nucl Chem* **1964**, *26*, 1927-1944.
[27] K. S. Rajan, A. E. Martell, *Inorg Chem* **1965**, *4*, 462-469.
[28] G. Bombieri, F. Benetollo, A. Delpra, R. Rojas, *J Inorg Nucl Chem* **1979**, *41*, 201-203.
[29] G. Bombieri, F. Benetollo, R. M. Rojas, M. L. Depaz, *J Inorg Nucl Chem* **1981**, *43*, 3203-3207.
[30] G. Bombieri, F. Benetollo, R. M. Rojas, M. L. Depaz, A. Delpra, *Inorg Chim Acta* **1982**, *61*, 149-154.
[31] T. Loiseau, I. Mihalcea, N. Henry, C. Volkringer, *Coordin Chem Rev* **2014**, *266*, 69-109.
[32] A. Kirchon, L. Feng, H. F. Drake, E. A. Joseph, H. C. Zhou, *Chem Soc Rev* **2018**, *47*, 8611-8638.
[33] W. Xu, Y. N. Ren, M. Xie, L. X. Zhou, Y. Q. Zheng, *Dalton Trans* **2018**, *47*, 4236-4250.
[34] S. Pasquale, S. Sattin, E. C. Escudero-Adan, M. Martinez-Belmonte, J. de Mendoza, *Nat Commun* **2012**, *3*.
[35] K. Q. Hu, X. Jiang, C. Z. Wang, L. Mei, Z. N. Xie, W. Q. Tao, X. L. Zhang, Z. F. Chai, W. Q. Shi, *Chem-Eur J* **2017**, *23*, 529-532.
[36] P. Thuéry, *Chem Commun* **2006**, 853-855.
[37] P. Thuéry, Y. Atoini, J. Harrowfield, *Inorg Chem* **2019**, *58*, 6550-6564.

[38] P. Thuéry, E. Riviere, J. Harrowfield, *Cryst Growth Des* **2016**, *16*, 2826-2835.
[39] P. Thuéry, *Cryst Growth Des* **2016**, *16*, 546-549.
[40] P. Thuéry, Y. Atoini, J. Harrowfield, *Inorg Chem* **2019**, *58*, 567-580.
[41] P. Thuéry, J. Harrowfield, *Dalton Trans* **2017**, *46*, 13677-13680.
[42] P. Thuéry, J. Harrowfield, *Inorg Chem* **2015**, *54*, 10539-10541.
[43] L. A. Borkowski, C. L. Cahill, *Acta Crystallogr E* **2005**, *61*, M816-M817.
[44] L. A. Borkowski, C. L. Cahill, *Inorg Chem* **2003**, *42*, 7041-7045.
[45] L. A. Borkowski, C. L. Cahill, *Cryst Growth Des* **2006**, *6*, 2248-2259.
[46] J. Wang, Z. Wei, F. W. Guo, C. Y. Li, P. F. Zhua, W. H. Zhua, *Dalton Trans* **2015**, *44*, 13809-13813.
[47] J. Y. Kim, A. J. Norquist, D. O'Hare, *Dalton Trans* **2003**, 2813-2814.
[48] L. Natrajan, F. Burdet, J. Pecaut, M. Mazzanti, *J Am Chem Soc* **2006**, *128*, 7152-7153.
[49] K. R. Howes, A. Bakac, J. H. Espenson, *Inorg Chem* **1988**, *27*, 791-794.
[50] T. Privalov, P. Macak, B. Schimmelpfennig, E. Fromager, I. Grenthe, U. Wahlgren, *J Am Chem Soc* **2004**, *126*, 9801-9808.
[51] H. Steele, R. J. Taylor, *Inorg Chem* **2007**, *46*, 6311-6318.
[52] L. Chatelain, S. White, R. Scopelliti, M. Mazzanti, *Angew Chem Int Edit* **2016**, *55*, 14323-14327.
[53] V. Mougel, P. Horeglad, G. Nocton, J. Pecaut, M. Mazzanti, *Angew Chem Int Edit* **2009**, *48*, 8477-8480.
[54] J. C. Sullivan, A. J. Zielen, J. C. Hindman, *J Am Chem Soc* **1961**, *83*, 3373-3378.
[55] I. Mihalcea, N. Henry, N. Clavier, N. Dacheux, T. Loiseau, *Inorg Chem* **2011**, *50*, 6243-6249.
[56] J. Lhoste, N. Henry, P. Roussel, T. Loiseau, F. Abraham, *Dalton Trans* **2011**, *40*, 2422-2424.
[57] R. C. Severance, M. D. Smith, H. C. zur Loye, *Inorg Chem* **2011**, *50*, 7931-7933.
[58] P. M. Cantos, L. J. Jouffret, R. E. Wilson, P. C. Burns, C. L. Cahill, *Inorg Chem* **2013**, *52*, 9487-9495.
[59] P. O. Adelani, P. C. Burns, *Inorg Chem* **2012**, *51*, 11177-11183.
[60] S. W. Buckner, J. R. Gord, B. S. Freiser, *J Am Chem Soc* **1988**, *110*, 6606-6612.
[61] K. A. Zemski, D. R. Justes, A. W. Castleman, *J Phys Chem B* **2002**, *106*, 6136-6148.
[62] J. N. Harvey, R. Poli, K. M. Smith, *Coordin Chem Rev* **2003**, *238*, 347-361.
[63] R. A. J. O'Hair, *Chem Commun* **2006**, 1469-1481.
[64] Y. Sevryugina, A. Y. Rogachev, M. A. Petrukhina, *Inorg Chem* **2007**, *46*, 7870-7879.
[65] L. Duchackova, D. Schroder, J. Roithova, *Inorg Chem* **2011**, *50*, 3153-3158.
[66] N. Dietl, M. Schlangen, H. Schwarz, *Angew Chem Int Edit* **2012**, *51*, 5544-5555.
[67] R. A. J. O'Hair, A. Mravak, M. Krstic, V. Bonacic-Koutecky, *ChemCatChem* **2019**, *11*, 2443-2448.
[68] D. Rios, M. D. Micheini, A. F. Lucena, J. Marçalo, J. K. Gibson, *J Am Chem Soc* **2012**, *134*, 15488-15496.
[69] Y. Gong, W. A. de Jong, J. K. Gibson, *J Am Chem Soc* **2015**, *137*, 5911-5915.
[70] P. D. Dau, P. V. Dau, L. F. Rao, A. Kovacs, J. K. Gibson, *Inorg Chem* **2017**, *56*, 4186-4196.
[71] H. S. Hu, J. Jian, J. Li, J. K. Gibson, *Inorg Chem* **2019**, *58*.
[72] S. O. Odoh, N. Govind, G. Schreckenbach, W. A. de Jong, *Inorg Chem* **2013**, *52*, 11269-11279.
[73] R. L. Feng, E. D. Glendening, K. A. Peterson, *Phys Chem Chem Phys* **2019**, *21*, 7953-7964.
[74] D. Rios, M. C. Michelini, A. F. Lucena, J. Marçalo, T. H. Bray, J. K. Gibson, *Inorg Chem* **2012**, *51*, 6603-6614.
[75] D. Rios, P. X. Rutkowski, D. K. Shuh, T. H. Bray, J. K. Gibson, M. J. Van Stipdonk, *J Mass Spectrom* **2011**, *46*, 1247-1254.
[76] S. Gronert, *J Am Soc Mass Spectr* **1998**, *9*, 845-848.
[77] D. M. D'Alessandro, F. R. Keene, *Chem Soc Rev* **2006**, *35*, 424-440.
[78] P. Verma, R. Maurice, D. G. Truhlar, *J Phys Chem C* **2015**, *119*, 28499-28511.
[79] M. J. Frisch, G. W. Trucks, H. B. Schlegel, G. E. Scuseria, M. A. Robb, J. R. Cheeseman, G. Scalmani, V. Barone, B. Mennucci, G. A. Petersson, H. Nakatsuji, M. Caricato, X. Li, H. P. Hratchian, A. F.

Izmaylov, J. Bloino, G. Zheng, J. L. Sonnenberg, M. Hada, M. Ehara, K. Toyota, R. Fukuda, J. Hasegawa, M. Ishida, T. Nakajima, Y. Honda, O. Kitao, H. Nakai, T. Vreven, J. A. Montgomery, Jr., J. E. Peralta, F. Ogliaro, M. Bearpark, J. J. Heyd, E. Brothers, K. N. Kudin, V. N. Staroverov, R. Kobayashi, J. Normand, K. Raghavachari, A. Rendell, J. C. Burant, S. S. Iyengar, J. Tomasi, M. Cossi, N. Rega, J. M. Millam, M. Klene, J. E. Knox, J. B. Cross, V. Bakken, C. Adamo, J. Jaramillo, R. Gomperts, R. E. Stratmann, O. Yazyev, A. J. Austin, R. Cammi, C. Pomelli, J. W. Ochterski, R. L. Martin, K. Morokuma, V. G. Zakrzewski, G. A. Voth, P. Salvador, J. J. Dannenberg, S. Dapprich, A. D. Daniels, O. Farkas, J. B. Foresman, J. V. Ortiz, J. Cioslowski, D. J. Fox, Gaussion, Inc., Wallingford, CT, **2009**.

[80] J. P. Perdew, M. Ernzerhof, K. Burke, *J Chem Phys* **1996**, *105*, 9982-9985.

[81] C. Adamo, V. Barone, *J Chem Phys* **1999**, *110*, 6158-6170.

[82] R. Maurice, E. Renault, Y. Gong, P. X. Rutkowski, J. K. Gibson, *Inorg Chem* **2015**, *54*, 2367-2373.

[83] P. D. Dau, R. Maurice, E. Renault, J. K. Gibson, *Inorg Chem* **2016**, *55*, 9830-9837.

[84] X. Y. Cao, M. Dolg, H. Stoll, *J Chem Phys* **2003**, *118*, 487-496.

[85] X. Y. Cao, M. Dolg, *J Mol Struc-Theochem* **2004**, *673*, 203-209.

[86] F. Weigend, R. Ahlrichs, *Phys Chem Chem Phys* **2005**, *7*, 3297-3305.

[87] D. Rappoport, F. Furche, *J Chem Phys* **2010**, *133*.

[88] V. Vallet, B. Schimmelpfennig, L. Maron, C. Teichteil, T. Leininger, O. Gropen, I. Grenthe, U. Wahlgren, *Chem Phys* **1999**, *244*, 185-193.

[89] V. Vallet, Y. Gong, M. Saab, F. Real, J. K. Gibson, *Dalton Trans* **2020**, *49*, 3293-3303.

[90] M. B. Robin, P. Day, in *Advances in Inorganic Chemistry and Radiochemistry, Vol. 10* (Eds.: H. J. Emeleus, A. G. Sharpe), Academic Press, New York, **1967**, pp. 247-422.

[91] C. R. Graves, J. L. Kiplinger, *Chem Commun* **2009**, 3831-3853.

[92] G. S. Groenewold, J. Oomens, W. A. de Jong, G. L. Gresham, M. E. McIlwain, M. J. Van Stipdonk, *Phys Chem Chem Phys* **2008**, *10*, 1192-1202.

[93] W. A. de Jong, E. Apra, T. L. Windus, J. A. Nichols, R. J. Harrison, K. E. Gutowski, D. A. Dixon, *J Phys Chem A* **2005**, *109*, 11568-11577.

[94] G. S. Groenewold, W. A. de Jong, J. Oomens, M. J. Van Stipdonk, *J Am Soc Mass Spectr* **2010**, *21*, 719-727.

[95] O. P. Lam, F. W. Heinemann, K. Meyer, *Chem Sci* **2011**, *2*, 1538-1547.

[96] C. J. Cramer, W. B. Tolman, K. H. Theopold, A. L. Rheingold, *P Natl Acad Sci USA* **2003**, *100*, 3635-3640.

[97] A. F. Lucena, J. M. Carretas, J. Marçalo, M. C. Michelini, Y. Gong, J. K. Gibson, *J Phys Chem A* **2015**, *119*, 3628-3635.

[98] F. Liu, J. J. Concepcion, J. W. Jurss, T. Cardolaccia, J. L. Templeton, T. J. Meyer, *Inorg Chem* **2008**, *47*, 1727-1752.